How shunting inhibition affects the discharge of lumbar motoneurones: a dynamic clamp study in anaesthetized cats

L. Brizzi, C. Meunier, D. Zytnicki, M. Donnet, D. Hansel, B. Lamotte d'Incamps and C. van Vreeswijk

Neurophysique et Physiologie du Système Moteur, UMR 8119 CNRS, Université René Descartes, 45 rue des Saints Pères, 75270 Paris Cedex 06, France

In the present work, dynamic clamp was used to inject a current that mimicked tonic synaptic activity in the soma of cat lumbar motoneurones with a microelectrode. The reversal potential of this current could be set at the resting potential so as to prevent membrane depolarization or hyperpolarization. The only effect of the dynamic clamp was then to elicit a constant and calibrated increase of the motoneurone input conductance. The effect of the resulting shunt was investigated on repetitive discharges elicited by current pulses. Shunting inhibition reduced very substantially the firing frequency in the primary range without changing the slope of the current–frequency curves. The shift of the *I–f* curve was proportional to the conductance increase imposed by the dynamic clamp and depended on an intrinsic property of the motoneurone that we called the shunt potential. The shunt potential ranged between 11 and 37 mV above the resting potential, indicating that the sensitivity of motoneurones to shunting inhibition was quite variable. The shunt potential was always near or above the action potential voltage threshold. A theoretical model allowed us to interpret these experimental results. The shunt potential was shown to be a weighted time average of membrane voltage. The weighting factor is the phase response function of the neurone that peaks at the end of the interspike interval. The shunt potential indicates whether mixed synaptic inputs have an excitatory or inhibitory effect on the ongoing discharge of the motoneurone.

(Received 8 January 2004; accepted after revision 23 May 2004; first published online 28 May 2004)
Corresponding author D. Zytnicki: Neurophysique et Physiologie du Système Moteur, UMR 8119 CNRS, Université René Descartes, 45 rue des Saints Pères, 75270 Paris Cedex 06, France. Email: daniel.zytnicki@univ-paris5.fr

Early work in cat lumbar motoneurones demonstrated that the increase in membrane conductance induced by inhibitory synapses is a key factor in their mode of operation (Coombs *et al.* 1955*b*). The shunting effect of inhibitory synapses was shown to reduce the amplitude of excitatory potentials, adding to the effect of membrane hyperpolarization. Inhibitory synaptic activity induced by repetitive electrical stimulation of hindlimb afferents can increase the conductance at the soma by more than 50% (Schwindt & Calvin, 1973*a*). During fictive locomotion (Shefchyk & Jordan, 1985; Gosnach *et al.* 2000) and fictive scratching (Perreault, 2002) conductance increases of 25–100% were reported. However, the impact of the synaptic shunt on the discharge has never been clarified. Tonic activation of synapses was shown to shift the current–frequency relationship (*I–f* curve) of the motoneurone (obtained by measuring the stationary discharge frequencies elicited by depolarizing current pulses injected at the soma, Granit *et al.* 1966*a*; see also Powers & Binder, 1995), but we do not know whether the shunt by itself contributes to the shift of the *I–f* curve. Can it substantially lower the discharge frequency of motoneurones? Is such a shunting inhibition the main operating mode of inhibitory synapses?

The aim of the present work was to quantify the effect of a 10–100% increase in the input conductance on the repetitive discharge of lumbar motoneurones and to understand which intrinsic properties of motoneurones determine the magnitude of shunting inhibition. Our study relied on dynamic clamp (Robinson & Kawai, 1993; Sharp *et al.* 1993), which allowed us to investigate the effect of conductance increases alone without associated changes in membrane potential.

We imposed constant conductance increases rather than noisy inputs because the large and long lasting afterhyperpolarization of motoneurones makes their discharge quite regular and little sensitive to noise (see Powers & Binder, 2001). As in other neurones (Chance

 DOI: 10.1113/jphysiol.2003.059964

et al. 2002; Mitchell & Silver, 2003; Ulrich, 2003) and as expected from theoretical work (Holt & Koch, 1997; Capaday, 2002; Shriki *et al.* 2003), we found that, in motoneurones, a constant conductance increase shifted the current–frequency curve without changing its slope. Measurements of the shift allowed us to quantify the effect of shunting inhibition. We found that sensitivity to shunting inhibition was different among motoneurones, and we investigated the causes of such a differential sensitivity.

Preliminary results were presented in an abstract (Brizzi *et al.* 2001).

Methods

Animal preparation

Experiments were carried out on adult cats (2.6–3.2 kg) deeply anaesthetized with either sodium pentobarbitone (Pentobarbital, Sanofi, 4 cats) or α-chloralose (4 cats) in accordance with French legislation. In the former case anaesthesia was induced with an I.P. injection (45 mg kg^{-1}) supplemented whenever necessary by I.V. injections (3.6 mg kg^{-1}). In the latter case anaesthesia was induced by inhalation of 4–5% halothane (Laboratoire Belamont) in air and continued during surgery by inspiration through a tracheal canula of 1.5–2.5% halothane in a mixture of air (2 l min^{-1}) and O_2 (2 l min^{-1}). After the laminectomy, gas anaesthesia was replaced by chloralose anaesthesia (initial dose of 50–70 mg kg^{-1} I.V. supplemented by additional doses of 15–20 mg kg^{-1} when necessary). Animals were always paralysed with pancuronium bromide (Pavulon, Organon SA) at a rate of 0.4 mg h^{-1} and artificially ventilated (end-tidal P_{CO_2} maintained around 4%). A bilateral pneumothorax prevented movements of the rib cage. The adequacy of anaesthesia was assessed by myotic pupils associated with stability of blood pressure (measured in the carotid) and of heart rate. At the onset of an experiment, amoxicillin (Clamoxyl, Merieux, 500 mg) and methylprenidsolone (Solu-Medrol, Pharmacia, 5 mg) were given subcutaneously to prevent the risk of infection and oedema, respectively. The central temperature was kept at 38°C. Blood pressure was maintained above 90 mmHg by infusion of a 4% glucose solution containing $NaHCO_3$ (1%) and gelatin (14% Plasmagel, Roger Bellon) at a rate of 3–12 ml h^{-1}. A catheter allowed evacuation of urine from the bladder. At the end of the experiments, animals were killed with a lethal intravenous injection of pentobarbitone (250 mg).

The following nerves were cut, dissected and mounted on a pair of stimulating electrodes to identify recorded motoneurones: posterior biceps and semitendinosus (PBSt) taken together, gastrocnemius medialis together with gastrocnemius lateralis and soleus (triceps surae, TS), the remaining part of the tibialis nerve (Tib) and the common peroneal nerve (CP). In one experiment, the whole tibialis and common peroneal nerves were stimulated together ('sciatic'). The lumbosacral spinal segments were exposed by laminectomy, and the tissues in hindlimb and spinal cord were covered with pools of mineral oil kept at 38°C. Identification of the motoneurone species relied on the observation of an antidromic action potential in response to nerve stimulation. Axonal conduction time from the stimulating electrode and amplitude of the action potential were measured. The conduction length for each nerve was measured after the animal was killed, which allowed us to compute the axonal conduction velocity for each motoneurone.

Microelectrodes

It was crucial that microelectrodes (3 M KCl, tip diameter 2–2.5 μm, resistance 2–4 MΩ) used for intracellular recording of motoneurones did not polarize during injection of large currents. They were systematically tested within the spinal cord (tip at about 1 mm depth). Those displaying rectification during the injection of a 40 nA depolarizing current (700 ms duration pulse) were discarded. Diffusion of chloride ions from the microelectrode to the neurone could slightly hyperpolarize the membrane potential. In all cases we started recordings only after the resting potential had settled to a constant stable value.

The dynamic clamp method

Dynamic clamp allows one to investigate the effects of passive membrane conductance increases on the firing properties of neurones (Manor *et al.* 2000; Cymbalyuk *et al.* 2002). We used this method here to mimic the repetitive and asynchronous activation of numerous inhibitory synapses at the soma. In this situation the total synaptic conductance is constant in average and displays small fluctuations. Therefore, at each time point we injected, through the microelectrode, the current:

$$I(t) = G_{\mathrm{syn}}[E_{\mathrm{rev}} - V(t)]$$

where $V(t)$ was the membrane potential, G_{syn} (μS) the constant synaptic conductance and E_{rev} (mV) the reversal potential. The conductance and the reversal potential were chosen independently. The conductance achieved its constant value instantaneously when the dynamic clamp was switched on.

Our dynamic clamp protocol amounts to the feedback loop sketched in Fig. 1*A*. The membrane potential, recorded either in the discontinuous current clamp or bridge mode (see below) of an Axoclamp 2B amplifier (Axon Instruments), was digitized at 10 kHz by the analog-to-digital converter of a Power 1401 unit (Cambridge Electronic Design Instruments) under the control of a PC computer running Spike2 software. The membrane potential was then filtered using a first-order, low-pass filter with a time constant of 1.6 ms. This was necessary to avoid oscillatory instabilities in the feedback loop when conductance increases comparable to

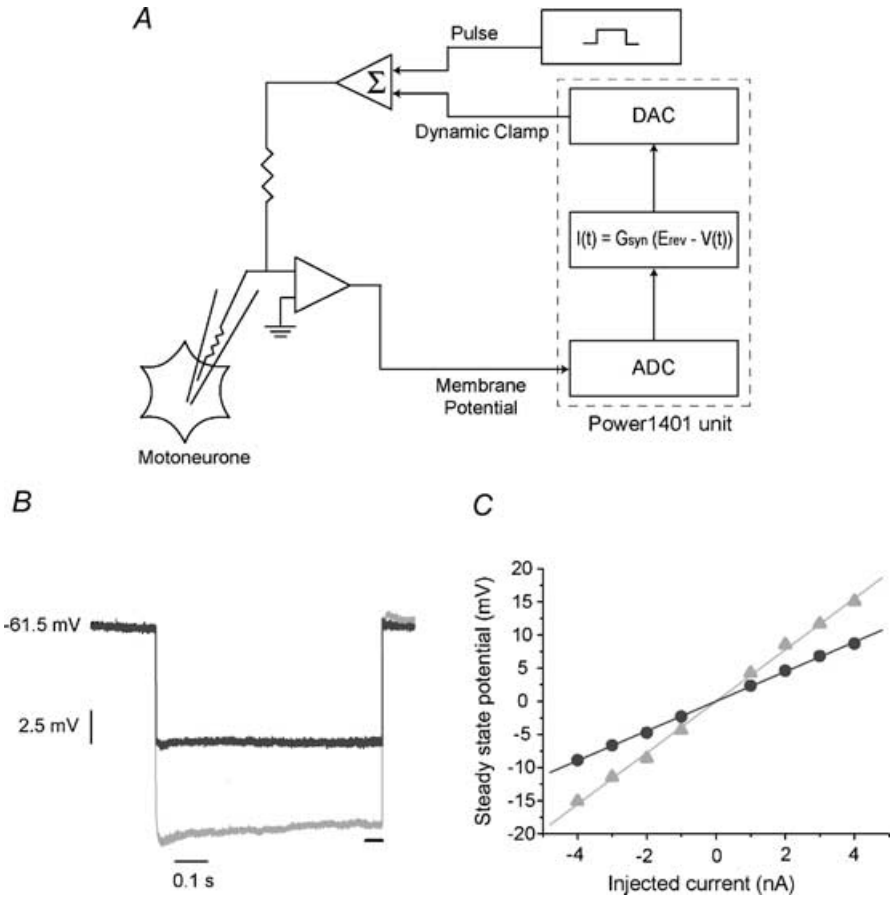

Figure 1. Increase of the motoneurone input conductance imposed by the dynamic clamp
A, schematic diagram of the experimental set-up for dynamic clamp. Repetitive firing of the motoneurone was elicited by an intracellular current pulse generated with the step command of the Axoclamp 2B amplifier. The membrane potential was digitized with an analog-to-digital converter (ADC) and low-pass filtered (see text). For each value of the membrane potential, the Power 1401 unit computed the current to be injected into the motoneurone through the intracellular microelectrode. This current was then converted into a voltage by a digital-to-analog converter (DAC). The resulting clamp signal was fed into the current injection circuit of the Axoclamp 2B amplifier where it was added to the current pulse. *B*, voltage response of a common peroneal motoneurone to a 4 nA hyperpolarizing current pulse of 700 ms duration. Responses (average of 4 successive records) without (grey trace) and with the dynamic clamp feedback (black trace, $G_{syn} = 0.2\ \mu S$). The plateau response was defined as the difference between the resting potential and the mean voltage during the last 0.5 s (horizontal bar below the trace). In the dynamic clamp condition, the plateau response was reduced by 44%. Note that the voltage sag was particularly small in this motoneurone (sag conductances contributed only 8% to the input conductance) and almost disappeared in the dynamic clamp condition. *C*, same motoneurone as in *B*. *V–I* curves obtained without (grey triangles) and with (black circles) dynamic clamp feedback imposing a 0.2 μS increase of the input conductance. Regression lines superimposed. Voltages were computed during the plateau (see *B*). Therefore, the slope of the regression line gives the sum of the passive input conductance and of the sag conductance. As expected, the slope of the *V–I* curve decreased from 3.9 to 2.2 MΩ (0.25 and 0.45 μS input conductance, respectively). Note that, for the small currents injected, *V–I* curves did not significantly depart from linearity. This was also the case for the other recorded motoneurones, though they exhibited larger voltage sags.

the resting input conductance were imposed. The time constant of the filter was much shorter than the decay rate of afterhyperpolarization so that the filtered voltage faithfully followed the membrane voltage *between* spikes. We always used this filtered voltage to compute the current injected through the microelectrode. Filtering had some effect on the shape of recorded action potentials, but we checked that this had a negligible impact on the steady-state firing rate, the spike duration being short compared to the interspike interval. Calculation of the injected current was performed online using the processor of the Power 1401 unit. The result of this computation was converted into a voltage by the digital-to-analog converter included in the Power 1401 unit and used to drive current injection through the microelectrode.

The sequencer of the Power 1401 unit processed one instruction every 10 μs. Computing the injected current required nine instructions and took 90 μs. This allowed us to set the sampling period of the membrane potential at 100 μs and to complete all computations for a given voltage before the next sampling. Discontinuous current clamp is the recommended mode for dynamic clamp (see Prinz *et al.* 2004) and was often used in *in vitro* experiments (see for instance Sharp *et al.* 1993; Le Masson *et al.* 2002; Cymbalyuk *et al.* 2002). It gives reliable records of the membrane potential, even while injecting a large current through the microelectrode. In most motoneurones (15 out of 19), the membrane potential was recorded using this mode at a sampling rate of 10 kHz, i.e. a frequency compatible with dynamic clamp. In the four remaining neurones the membrane potential was recorded using the bridge mode. This mode could be used only if the microelectrode resistance did not change during the recording session. Bridge compensation for the microelectrode resistance was done before motoneurone impalement. We checked after withdrawal of the microelectrode from the motoneurone that its resistance had not changed.

Setting the reversal potential to the resting potential (V_{rest}) allowed us to increase the input conductance without altering the resting potential and to investigate the effect of the shunt *per se*. As long as the motoneurone was at rest, no current passed through the microelectrode. When the motoneurone was depolarized by a current step (see below), and when it fired, the dynamic clamp generated a negative current, $I(t) = G_{\text{syn}}[V_{\text{rest}} - V(t)]$, proportional to the conductance we imposed.

Experimental protocol

A typical recording sequence ran as follows. We first recorded the voltage responses to a series of hyperpolarizing and depolarizing current pulses (1–4 nA intensity and 700 ms duration) repeated at the rate of 0.5 Hz. This was done with and without shunt in order to compute the input conductance in both conditions (see next paragraph). Then depolarizing pulses were used to determine the threshold current for repetitive firing. Finally, a series of depolarizing current pulses (700 ms duration) ranging from 5 to 40 nA repeated with a frequency of 0.5 Hz and increased by steps of 1–5 nA were used to determine the current–frequency curves. For each step, 5–10 successive trials were recorded without and then with 'synaptic' shunt. When possible, several values of the imposed conductance were tested either in increasing or decreasing order. Results did not depend on the order.

Offline data analysis

The voltage responses were averaged for each subthreshold current step. A sag of the membrane potential was often observed during hyperpolarizing (see Fig. 1*B*) or depolarizing pulses (Nelson & Frank, 1967; Gustafsson & Pinter, 1984). We used the plateau of the response to compute the input conductance (Schwindt, 1973). The input conductance therefore included the contribution of the active conductances responsible for the sag. This contribution amounted to 8–47% (mean = 24%, S.D. = 10%) of the input conductance. As illustrated in Fig. 1*B* (compare black and grey traces), switching on the dynamic clamp decreased the voltage response. The change in slopes of *V*–*I* curves in Fig. 1*C* shows that the input conductance of this motoneurone increased from 0.25 to 0.45 μS: the 0.2 μS conductance imposed by the dynamic clamp simply added to the input conductance. This is the expected result for synaptic inputs at the soma.

Steady-state *I*–*f* curves (see Fig. 3) were plotted as follows. To compute the mean stationary frequency over as many spikes as possible we used the whole 'adapted' discharge. This required us to discard the first two or three spikes (depending on the motoneurone) because they corresponded to the initial adaptation phase of the discharge. For each pulse intensity and synaptic conductance, the 5–10 trials performed were then pooled together and the mean and standard deviation of the instantaneous frequency in the steady-state regime were computed using the Spike2 software.

Statistical analysis

We did not compute *separately* the regression lines for the different shunting conditions because this method was not appropriate to check that shunting inhibition

shifted the *I–f* curve of a motoneurone proportionaly to the imposed conductance. Instead we tried to account *simultaneously* for all the current–frequency curves of a given motoneurone. To test whether shunting inhibition changed the slope or not and to assess whether the shift was proportional to the imposed conductance, we used the *quadratic* model: $f = c_1 + c_2 I + c_3 G_{syn} + c_4 I G_{syn} + c_5 G^2_{syn}$ (see Graybill, 1961). In this model, f was the steady-state firing frequency, I the intensity of the current pulse, and the free parameters $c_1 - c_5$ were determined by data fitting. In all motoneurones, both c_4 and c_5 were found to be close to zero, indicating that shunting inhibition did not significantly change the slope of the current–frequency curve and that the shift was proportional to G_{syn}. This suggested that a simpler *multilinear* model where $f = c_1 + c_2 I + c_3 G_{syn}$ was sufficient to account for the data. We verified this point using the Fisher F test and found that indeed the quadratic model did not fit our data better than the linear model. Finally the χ^2 test showed that the multilinear model provided a good fit, and we therefore used this model to determine the slope and the shift of the *I–f* curves.

Results

We report data from 19 lumbar motoneurones (8 CP, 3 TS, 3 Tib, 1 PBSt and 4 sciatic). These neurones were selected because their resting membrane potential was between −80 and −51 mV, and the amplitude of their antidromic action potential was in the 70−95 mV range, indicating good microelectrode penetration. In addition, these conditions remained stable (with variations not larger than 3 mV) during the whole recording sequence that lasted at least half an hour. Threshold currents for repetitive firing were in the 5–21 nA range. Input conductances ranged from 0.26 to 1.89 μS. Imposed shunting conductances in the 0.1–0.5 μS range increased the input conductances by 6–109%. No systematic difference was seen between pentobarbitone and α-chloralose experiments, and between bridge and DCC recording modes. Therefore the results were pooled together. Setting the reversal potential to the resting potential in the dynamic clamp equation (see Fig. 1*A*) and varying the imposed shunting conductance enabled us to determine in 16 motoneurones how the shunt effect changed the steady-state current–frequency curve. In the three remaining neurones we varied both the imposed

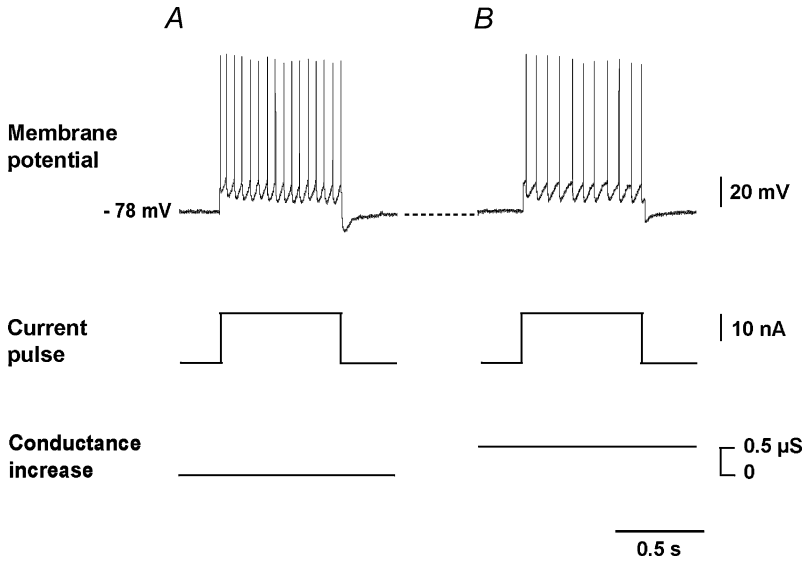

Figure 2. How a conductance increase affects the firing rate
Comparison between the control condition (*A*) and a dynamic clamp condition where $G_{syn} = 0.5$ μS (*B*). Upper traces, membrane potential; middle traces, current pulse; lower traces, extra conductance imposed by the dynamic clamp. Increasing the input conductance via the dynamic clamp did not affect the resting membrane potential, which remained at −78 mV (*B*, upper trace). Therefore the reduction of the firing rate followed only from the input conductance increase, i.e. from shunting inhibition. Note that the hyperpolarization after the end of the pulse was smaller in *B* than in *A* because (i) the last spike occurred 20 ms earlier in *B* than in *A*, so that by the end of the pulse, afterhyperpolarization had partially relaxed, and (ii) the larger membrane conductance in *B* reduced the amplitude of afterhyperpolarization. Records from a sciatic motoneurone with an input conductance of 1.56 μS in the absence of dynamic clamp (condition *A*).

conductance and the reversal potential and investigated how this modified the firing frequency for a given value of the injected current.

Shunting inhibition shifted the *I–f* curve proportionally to the imposed conductance

Figure 2 illustrates how increasing the input conductance affects the discharge of motoneurones. A depolarizing current pulse of 20 nA induced repetitive firing. In the control condition (Fig. 2*A*), the frequency settled at 21 Hz after a brief adaptation period. We then imposed a 0.5 μS conductance increase via the dynamic clamp, which changed the input conductance by 32%. This slowed the firing rate down to 14 Hz for the same intensity of the current pulse (Fig. 2*B*). The resting membrane potential was the same in both conditions (−78 mV). The dynamic clamp method thus allowed us to create an artificial shunting 'synapse' that reduced the firing rate of the motoneurone. In other words, we elicited shunting inhibition.

The effect of the shunting conductance was qualitatively the same in the 16 motoneurones for which we computed steady-state *I–f* curves: it shifted the curves to the right without changing their slope. This is illustrated in Fig. 3 for two motoneurones. For the motoneurone of Fig. 3*A*, four shunting conditions were investigated. The shift was proportional to the imposed conductance. A shunting conductance of 0.1 μS, which increased the input conductance by only 11%, already shifted the *I–f* curve by 3.2 nA. For the largest tested value (0.3 μS), the shift reached 9.6 nA, and firing frequency was reduced by about 9 Hz whatever the intensity of the current pulse. Qualitatively similar results were obtained for the motoneurone of Fig. 3*B*, the only one in our sample that displayed voltage threshold accommodation (Schwindt & Crill, 1982). The accommodation rate was the same in the control and shunting conditions (0.3 mV nA^{-1}). In

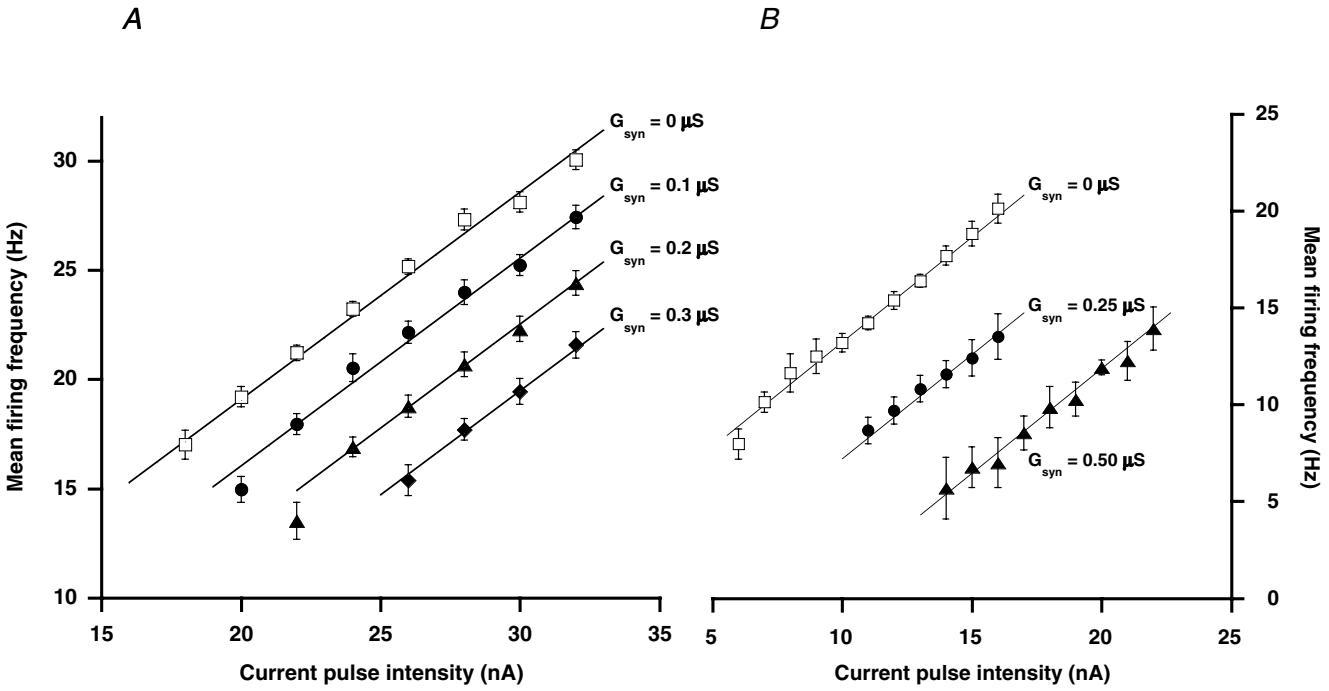

Figure 3. Effect of shunting inhibition on *I–f* curves

I–f curves in control (open squares) and several shunting conditions (filled symbols). Each symbol represents the mean instantaneous frequency in the steady-state regime for a given value of the injected current, the associated vertical bar indicating the standard deviation. Multilinear regression lines (see Methods) are also displayed. *A*, CP motoneurone with an input conductance of 0.89 μS. Three shunting conditions were investigated: $G_{syn} = 0.1$ μS (circles), 0.2 μS (triangles), and 0.3 μS (diamonds). *B*, TS motoneurone with an input conductance of 0.46 μS. This motoneurone was the only one in our sample that displayed voltage threshold accommodation. Two shunting conditions were investigated: $G_{syn} = 0.25$ μS (circles), and $G_{syn} = 0.5$ μS (triangles). In both motoneurones, the conductance increase shifted the curves without altering their slope, and the shift was proportional to G_{syn}. Note that in dynamic clamp conditions we did not try to adjust the injected current to reach the minimum firing frequency.

this motoneurone, 0.25 and 0.5 μS shunting conductances increased the input conductance by 54 and 109%, shifting the *I–f* curves by 5.8 and 11.6 nA, respectively, without any significant change of slope. In all cells, the statistical analysis (see Methods) confirmed that increasing the input conductance shifted the current–frequency curve without affecting its slope. In 11 of 16 motoneurones the steady-state *I–f* curves were obtained for at least two values of the shunting conductance in addition to the control condition (no shunting conductance). This allowed us to verify that the shift of the curve was proportional to the shunting conductance. This linear dependence was found even when the shunting conductance was as large as the input conductance of the neurone (see Fig. 3*B*). Shunting inhibition thus had the same effect as the injection of a constant hyperpolarizing current, independent of the membrane potential and linearly increasing with the shunting conductance.

Sensitivity to shunting and shunt potential of motoneurones

The shift of the *I–f* curve was equal to the shunting conductance times a coefficient that depended only on the intrinsic properties of the motoneurone. This coefficient had the dimension of a potential (mV) and could be written as $V_{\text{shunt}} - V_{\text{rest}}$, where V_{shunt} was a potential that we called the shunt potential of the cell. The shunt potential determined the shift of the current–frequency curve, equal to $G_{\text{syn}}(V_{\text{shunt}} - V_{\text{rest}})$, for any value of the shunting conductance, hence its name (see next section and Fig. 4 for a more direct definition of the shunt potential).

The statistical error in the quantity $V_{\text{shunt}} - V_{\text{rest}}$ was smaller than 2 mV in 9 of 16 motoneurones. For these motoneurones, the quantity $V_{\text{shunt}} - V_{\text{rest}}$ ranged from 14 to 37 mV (mean = 25 mV, S.D. = 8 mV). This showed that shunting inhibition did not have the same impact on all motoneurones. We could not detect any correlation between the sensitivity to shunting inhibition, measured by $V_{\text{shunt}} - V_{\text{rest}}$, and the motoneurone identity, its input conductance at soma, the slope of its *I–f* curve, or its axonal conduction velocity. But the lack of correlation could be due to the small size ($N = 9$) of our sample.

The shunt potential could be directly measured

Real synapses do not act only through their shunt effect since their reversal synaptic potential generally differs from the resting membrane potential. When the reversal potential is below the resting potential, the synapse, in addition to increasing the membrane conductance, elicits a negative current that hyperpolarizes the membrane. This current by itself reduces the firing frequency and *adds* to the effect of the shunt. Conversely, when the reversal potential is above the resting potential a depolarizing current results that increases the firing frequency and *competes* with shunting inhibition. Using the dynamic clamp in three motoneurones, we determined for which values of the reversal potential the shunt effect prevailed over the depolarization. Figure 4 shows the results obtained in one of these motoneurones, whose resting membrane potential was −77 mV. When the reversal potential was set at −70 mV the shunt effect predominated: despite the depolarization of the membrane, increasing the imposed shunting conductance *decreased* the firing rate. For instance, setting the shunting conductance to 0.2 μS, that is, increasing the input conductance by 30%, reduced the firing rate from 27 to 20 Hz. Inhibition decreased with increasing reversal potential, and for a specific value of the reversal potential (−60 mV for this neurone), changing the shunting conductance no longer had any effect on the discharge frequency. For higher values

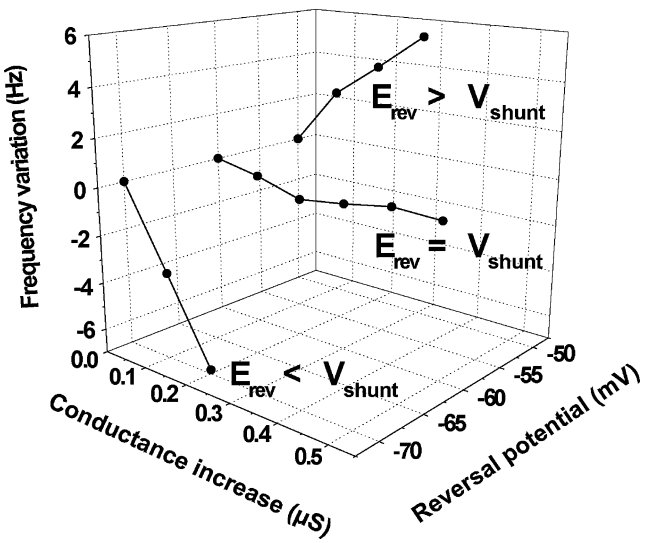

Figure 4. Effect of the reversal potential on the discharge frequency

The 3D diagram shows how the discharge frequency was modified by the conductance increase for three values of the reversal potential (−70, −60 and −50 mV). A depolarizing current pulse (16 nA, 700 ms) was used to elicit firing. The ordinate is the variation of the discharge frequency with respect to the control condition (i.e. when $G_{\text{syn}} = 0$). For $E_{\text{rev}} = -60$ mV, increasing G_{syn} had almost no effect on the firing rate of the motoneurone. This value corresponds to the shunt potential. When the reversal potential was greater than the shunt potential, the net effect was excitatory (increase of the firing rate with the imposed conductance). In the opposite case the net effect was inhibitory (decrease of the firing rate). $V_{\text{rest}} = -77$ mV. Tib motoneurone with an input conductance of 0.67 μS.

of the reversal potential the firing rate *increased* with the shunting conductance, indicating that the depolarizing effect prevailed on shunting inhibition. The net effect on the discharge was then excitatory. Similar results were obtained for the other two neurones in which the same experiment was carried out.

The shunt potential is an intrinsic property of the motoneurone and is not related to any synaptic reversal potential. However, it coincides in the above protocol with the value of the reversal potential E_{rev} for which changing the input conductance has no effect on the firing frequency. Indeed, in this condition the depolarizing current $G_{\mathrm{syn}}(E_{\mathrm{rev}} - V_{\mathrm{rest}})$ counterbalanced the shift $-G_{\mathrm{syn}}(V_{\mathrm{shunt}} - V_{\mathrm{rest}})$ of the *I–f* curve elicited by shunting inhibition. The shunt potential was thus directly determined in the three motoneurones investigated. It was found to be equal to −60 mV (see Fig. 4), −40 mV and −45 mV.

The shunt potential can be interpreted as follows. It takes intermediate values between the typical reversal potentials of excitatory and inhibitory synapses and indicates whether mixed excitatory and inhibitory inputs will have a net excitatory or inhibitory effect on the firing frequency. The firing frequency will increase if the reversal potential of the *net synaptic current* is above the shunt potential. In contrast, the firing frequency will decrease if this reversal potential is below the shunt potential.

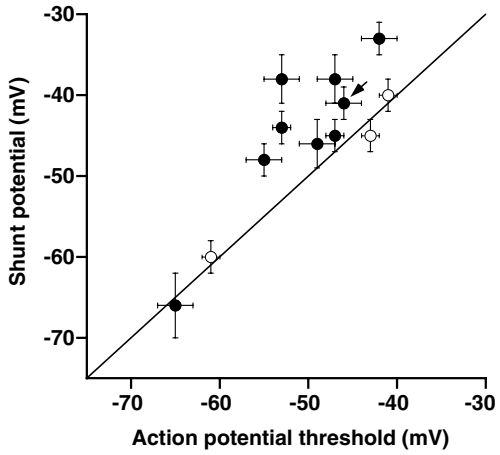

Figure 5. Relationship between the shunt potential and the action potential threshold

The shunt potential was directly measured for 3 motoneurones (open circles) and computed as explained in the text for the 9 other motoneurones (filled circles). The action potential threshold, defined as the voltage where the spike upstroke began, was determined by visual inspection in control conditions (no shunt) for the lowest injected current. This simple procedure proved to be more accurate than relying on the voltage derivative because of the noisiness of the traces. Vertical and horizontal bars indicate standard errors on the shunt potential and the action potential threshold, respectively. The error in the shunt potential takes into account both the statistical error in $V_{\mathrm{shunt}} - V_{\mathrm{rest}}$ and the uncertainty in the measurement of the resting potential. Errors in the action potential threshold arise from recording noise and variations of the threshold during the train. The oblique line is the bisectrix along which the shunt potential equals the action potential threshold. Measurements made in the accommodating motoneurone of Fig. 3*B* are indicated by the arrow.

Which cell property determines the shunt potential?

Pooling together the three motoneurones for which the shunt potential was directly measured (as in Fig. 4) and the nine motoneurones for which it could be computed from the shift of *I–f* curves, we obtained the values of the shunt potential shown in Fig. 5. The shunt potential is highly variable, lying between −66 and −33 mV (mean = −45 mV, S.D. = 9 mV). This is because the impact of a given synaptic current on the discharge depends on the response of the neuronal membrane, which varies from cell to cell.

Membrane responsiveness varies during the interspike interval and the effect of a given synaptic current is not the same at all times. The theoretical analysis detailed in Appendix shows that the shunt potential is a weighted average of the membrane potential given by the formula:

$$V_{\mathrm{shunt}} = \int_0^T V(t)Z(t)\,dt \Big/ \int_0^T Z(t)\,dt$$

In this formula, $Z(t)$ is the linear response function of the neurone (Hansel *et al.* 1993; Poliakov *et al.* 1997). It quantifies how a brief current pulse affects the discharge. We computed the shunt potential in a simple model of a motoneurone very similar to the one introduced by Baldissera *et al.* (1976). It turned out to be close to the action potential threshold (see Appendix). This prompted us to compare these two potentials in our sample of motoneurones. As shown in Fig. 5 (filled circles), the shunt potential was close to the action potential threshold, determined by visual inspection of records, for 6 of the 12 motoneurones (difference smaller than 3 mV) as predicted by the model. For the remaining motoneurones, the shunt potential was 5–15 mV above that threshold, that is, in the voltage range traversed during the rising phase of the spike. For these neurones, the effect of shunting inhibition was larger than expected from the simple model, suggesting that the active conductances involved in the action potential generation could enhance shunting inhibition. This point is further discussed in the Appendix. Altogether, our results indicate that the shunt potential is at least equal to the action potential threshold.

Discussion

The goal of the present study was to assess the quantitative effect of shunting inhibition on the current–frequency curves of cat motoneurones in the primary firing range. We showed that shunting inhibition could strongly reduce the firing frequency of lumbar motoneurones and had the same effect on the *I–f* curve as a constant hyperpolarizing current. This 'equivalent' current was proportional to the imposed shunting conductance and depended on an intrinsic property of the cell that we called its shunt potential. The shunt potential could be accurately determined in 12 neurones and was 11–37 mV above the resting potential. This spread indicated important differences in the sensitivity of motoneurones to shunting. The shunt potential was close to the spike voltage threshold in six motoneurones and 5–15 mV above this threshold for the other six neurones (including the motoneurone of Fig. 3*B* that displayed accommodation). These results were accounted for by the theoretical analysis presented in the Appendix. The shunt potential indicates whether mixed synaptic inputs will have a net excitatory or inhibitory effect on the ongoing discharge of the motoneurone.

Comparison with previous studies

Previous experimental studies, carried out on cats anaesthetized with barbiturates, demonstrated that tonic peripheral or descending synaptic inputs did not change the gain of motoneurones, i.e. the slope of their steady-state *I–f* curve, in the primary firing range (see the review of Powers & Binder, 2001). The curve was shifted to the left or the right depending on the balance between excitatory and inhibitory inputs. Similar conclusions were obtained in recent *in vitro* studies of cortical (Chance *et al.* 2002; Ulrich, 2003) and cerebellar neurones (Mitchell & Silver, 2003): noisy inputs changed the gain of the cell but a constant stimulation caused only a shift of the *I–f* curve.

Changes in the slope of *I–f* curves of motoneurones were observed in other experimental conditions. Granit *et al.* (1966*b*) argued that shifts of the *I–f* curves were limited to the primary firing range and that tonic synaptic activity could change the slope in the secondary range. We did not examine this issue. Our results were limited to the primary firing range because investigating the secondary range would have required large currents (greater than 40 nA). Such currents would have induced electrode polarization and could have caused a deterioration in the spiking mechanism because of long-lasting inactivation of the sodium current. Kernell (1966) observed an increase of the slope in the primary range during repetitive stimulation of the brainstem. This was associated with a decreased afterhyperpolarization probably due to neuromodulatory inputs. Similar effects were reported by Brownstone *et al.* (1992) during fictive locomotion in decerebrate cats. The slope of the current–frequency curve increased during episodes of locomotion and reverted to the control value when locomotion stopped. In contrast, Shapovalov & Grantyn (1968) observed that a repetitive stimulation of the reticular formation elicited either a simple shift of the *I–f* curve or a reduction of the slope in chromatolysed motoneurones.

It is widely believed that the shift of the *I–f* curve, elicited by tonic synaptic activation, is equal to the average synaptic current, acting at the soma (Powers & Binder, 1995; Holt & Koch, 1997; Ulrich, 2003), but this stems from a reasoning error. When the motoneurone discharges, intrinsic active conductances, such as the afterhyperpolarization conductance, vary during the interspike interval. They shape the voltage trajectory and the response of the membrane to synaptic inputs. In these conditions, the shift of *I–f* curves is determined by *both* the synaptic input and the membrane response function. The shift would be equal to the average synaptic current only if the response of the membrane was the same at all times, which is not true (see Fig. 6 in Appendix).

In our study, we focused on the sensitivity of motoneurones to shunting inhibition. Only one study has previously addressed this issue (Schwindt & Calvin, 1973*b*). The authors did not observe significant shifts of *I–f* curves when synaptic inputs elicited by an electrical stimulation of a hindlimb nerve increased the input conductance of lumbar motoneurones, by as much as 70%, with little effect on the resting membrane potential. The fact that *I–f* curves were not shifted might suggest that the shunt potential was close to the reversal potential of the net synaptic current and therefore near the resting membrane potential. However, we never observed such a situation in our experiments: the shunt potential was always close to the voltage threshold for spiking or above it, exceeding the resting potential by at least 11 mV.

Functional implications

Our results suggest that inhibitory synapses, which are mainly located on the soma or on proximal dendrites (see for instance Burke *et al.* 1971; Fyffe, 1991), largely act through their shunting inhibition. Indeed the efficacy of shunting inhibition is measured by $V_{\text{shunt}} - V_{\text{rest}}$, which ranged from 11 to 37 mV in the present study. This is about twice the driving force of inhibitory synapses, the reversal potential of which is 5–20 mV below the resting potential (Coombs *et al.* 1955*a*). The added effects of

the hyperpolarization and of the shunt endow inhibitory synapses with an efficacy comparable to that of excitatory synapses. Therefore, shunting inhibition is probably a major operating mode of the inhibitory systems acting on motoneurones (Ia reciprocal inhibition, Ib inhibition, recurrent inhibition, etc.).

Our results were obtained in motoneurones of anaesthetized animals. In these animals, the discharge of motoneurones is controlled by the slow after-hyperpolarization current. Responsiveness to synaptic inputs is high only near the end of the interval. This fully explains all observed features of shunting inhibition: the constancy of the slope of the *I–f* curve, the shift of the curve proportional to the shunting conductance, and a shunt potential close to the spike threshold or above it (see theoretical analysis in Appendix). Experiments in non-anaesthetized and decerebrated cats indicate that neuromodulatory inputs may place motoneurones in another state in which afterhyperpolarization is reduced and persistent inward currents are expressed (see, for instance, Hounsgaard *et al.* 1988; Brownstone *et al.* 1992; Bennett *et al.* 1998; and the review on this point in Powers & Binder, 2001). Both experimental and modelling studies have shown that reducing the conductance responsible for afterhyperpolarization increases the firing frequency of motoneurones and the slope of their current–frequency curve (Kernell, 1966; Kernell, 1968; Zhang & Krnjevic, 1987). However, we expect that the reduction of afterhyperpolarization conductance will have little impact on the shunt potential, because the response function will still peak at the end of the interspike interval. In contrast, the activation of persistent inward currents dramatically alters the excitability of motoneurones and thereby their response function. It is difficult to speculate on the impact of persistent inward currents on shunting inhibition, all the more as inhibitory synapses can reduce these currents (Hultborn *et al.* 2003; Kuo *et al.* 2003). The interplay between shunting inhibition and persistent inward currents largely remains to be explored.

Appendix

To understand how a constant shunting conductance affects the discharge of motoneurones in our experiments one must determine the response properties of the membrane. The impulse response $Z(t)$ tells us by how much a brief current pulse at time t shifts the spike train (Hansel *et al.* 1993). The effect of the shunting current is obtained by summing the effects of elementary impulses: the interspike intervals increase by $\Delta T = \int_0^T G_{\mathrm{syn}}[V_{\mathrm{rest}} - V(t)]Z(t)\,dt$. *A priori*, this linear summation holds true only when the shunting current is small. From the formula above, one deduces the variation of the firing frequency, $\Delta f = -\Delta T/T^2$, and the shift of the

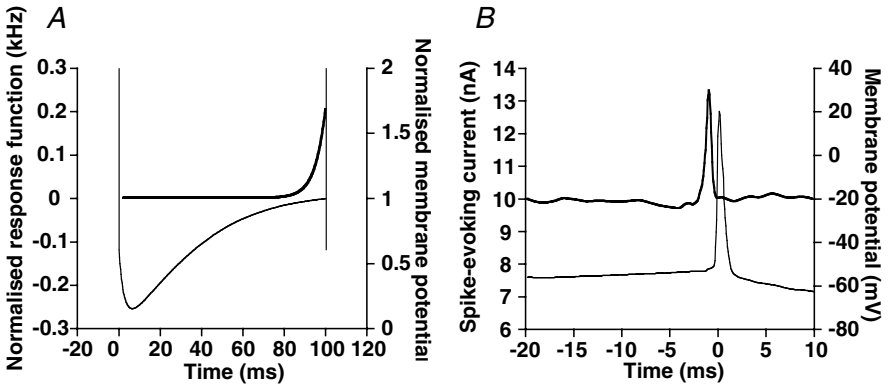

Figure 6. Response properties of an integrate-and-fire model (*A*) and of a cat lumbar motoneurone (*B*)
A, model described in Appendix. The resting potential is set to 0, the voltage threshold to 1, the reset potential following the spike to 0.6 and the Nernst potential of potassium to −1. Conductance of the slow after-hyperpolarization current following the first spike equals the input conductance. Passive membrane time constant, 5 ms; relaxation time constant of afterhyperpolarization, 25 ms; firing frequency, 10 Hz. Thick trace, normalized response function; thin trace, membrane potential normalized with respect to the action potential threshold. *B*, spike-evoking current (thick trace) and membrane potential (thin trace) as measured by Poliakov *et al.* (1997). A 10 nA current injected in the motoneurone elicited a repetitive discharge. Gaussian white noise was added to it and perturbed spike timing. The two traces were obtained by spike-triggered averaging. The linear response function is proportional to the spike evoking current minus the 10 nA baseline (see Poliakov *et al.* 1997).

I–f curve, $\Delta I = G_{syn} \int_0^T [V_{rest} - V(t)] Z(t)\, dt / \int_0^T Z(t)\, dt$. Comparison with the formula previously established, $\Delta I = G_{syn}(V_{rest} - V_{shunt})$, allows us to conclude that

$$V_{shunt} = \int_0^T V(t) Z(t)\, dt \Big/ \int_0^T Z(t)\, dt \qquad \text{(A1)}$$

This shows that the shunt potential is a weighted average of the membrane potential. The weighting factor is the normalized response function $Z(t)/\int_0^T Z(t)\, dt$.

We computed the response function of a single compartment integrate-and-fire model of the motoneurone (Kernell, 1968; Baldissera *et al.* 1976; C. Meunier & R. Borejsza, unpublished observations). The voltage evolution equation for this model reads

$$C_m \frac{dV(t)}{dt} = -G_m [V(t) - V_{rest}] + G_{AHP}(t) [V_K - V(t)] + I \qquad \text{(A2)}$$

where C_m is the membrane capacitance, G_m the passive conductance, G_{AHP} the conductance of the slow current responsible for afterhyperpolarization that exponentially decays, V_K the Nernst potential of potassium ions, and I the current pulse that elicits repetitive firing with period T. Every time the potential reaches the *fixed* spike threshold V_{th} an action potential is emitted, and voltage is reset to the value V_{reset}.

When a brief inhibitory current pulse $\delta I(t) = q\delta(t - t^*)$ delivers at time t^* a small negative charge q to the neurone, it produces a voltage drop, $\delta V(t^*) = q/C_m$. This voltage perturbation relaxes according to $C_m d\delta V/dt = -G(t)\delta V$ where $G(t) = G_m + G_{AHP}(t)$ is the membrane conductance at time t. At time T, a residual perturbation of the potential $\delta V(T) = \delta V(t^*) \exp[-\int_{t^*}^T dt'\, G(t')/C]$ is still present. As a consequence, the interspike interval is lengthened by the amount δT_1 that is computed by dividing $\delta V(T)$ by the time derivative of the voltage. The following intervals are also modified because lengthening an interval slightly decreases the AHP conductance in the next interval. After a while the discharge is again regular, but spikes are shifted by a quantity proportional to δT_1. This proves that $Z(t)$ is proportional to $\exp[-\int_t^T dt' G(t')/C]$.

The normalized response function is displayed in Fig. 6*A*. It is close to 0 on most of the interspike interval and it sharply rises near the end of the interval. This can be explained as follows. When a voltage perturbation occurs early in the interspike interval, it relaxes before the end of the interval and has a negligible effect on the timing of the next spike. In contrast, when the perturbation occurs at the end of the interval, the following spike is delayed until the perturbation has relaxed. Because our model is linear below the voltage threshold, the response function accounts for the effects of shunting currents even when the shunting conductance is comparable to the input conductance. The shift of the *I–f* curves is proportional to the shunting conductance and the shunt potential, computed from eqn (A1), is close to the voltage threshold. The model thus accounts for the linearity of the shift observed in all motoneurones of our sample and for the values of the shunt potential close to voltage threshold obtained in half of the motoneurones.

Because our model is restricted to the subthreshold voltage range and does not incorporate the currents responsible for action potentials, it cannot explain why the shunt potential was larger than the voltage threshold in the other half of our sample. Poliakov *et al.* (1997) determined experimentally the response function of cat lumbar motoneurones (see an example in Fig. 6*B*). It decays fast but not instantaneously to zero at the end of the interspike interval, in contrast to the model. Using the experimental response function (Fig. 6*B*), we computed the shunt potential from eqn (A1) and found $V_{shunt} \approx -52$mV, which was very close to the spike threshold potential measured on the voltage trace. This is because the decay phase of the response function does not overlap the rising phase of the action potential. A substantial overlap would much increase the product $V(t)Z(t)$, and would lead to shunt potentials well above the action potential threshold. We tested this idea by shifting to the right by 0.3 or 0.5 ms the response function of Fig. 6*B*. The shunt potential indeed increased by 3.5 and 11 mV, respectively. This suggests that small changes in the response properties of motoneurones may considerably increase V_{shunt} and explain the spread of the shunt potential observed in our sample, up to values 15 mV above the action potential threshold.

References

Baldissera F, Gustafsson B & Parmiggiani F (1976). A model for refractoriness accumulation and secondary range firing in spinal motoneurones. *Biol Cyber* **24**, 61–65.

Bennett DJ, Hultborn H, Fedirchuk B & Gorassini M (1998). Synaptic activation of plateaus in hindlimb motoneurones of decerebrate cats. *J Neurophysiol* **80**, 2023–2037.

Brizzi L, Hansel D, Meunier D, Van Vreeswijk C & Zytnicki D (2001). Shunting inhibition: a study using in vivo dynamic clamp on cat spinal motoneurons. *Soc Neurosci Abstr* **27**, 934.3.

Brownstone RM, Jordan LM, Kriellaars DJ, Noga BR & Schefchyk SJ (1992). On the regulation of repetitive firing in lumbar motoneurones during fictive locomotion in the cat. *Exp Brain Res* **90**, 441–455.

Burke RE, Fedina L & Lundberg A (1971). Spatial synaptic distribution of recurrent and group Ia inhibitory systems in cat spinal motoneurones. *J Physiol* **214**, 305–326.

Capaday C (2002). A re-examination of the possibility of controlling the firing gain of neurons by balancing excitatory and inhibitory conductances. *Exp Brain Res* **143**, 67–77.

Chance FS, Abbott LF & Reyes AD (2002). Gain modulation from background synaptic input. *Neuron* **35**, 773–782.

Coombs JS, Eccles JC & Fatt P (1955*a*). The specific ionic conductances and the ionic movements across the motoneuronal membrane that produce the inhibitory post-synaptic potential. *J Physiol* **130**, 326–373.

Coombs JS, Eccles JC & Fatt P (1955*b*). The inhibitory suppression of reflex discharges from motoneurones. *J Physiol* **130**, 396–413.

Cymbalyuk GS, Gaudry Q, Masino MA & Calabrese RL (2002). Bursting in leech heart interneurons: cell-autonomous and network-based mechanisms. *J Neurosci* **22**, 10580–10592.

Fyffe RE (1991). Spatial distribution of recurrent inhibitory synapses on spinal motoneurons in the cat. *J Neurophysiol* **65**, 1134–1149.

Gosnach S, Quevedo J, Fedirbuck B & McCrea DA (2000). Depression of group Ia monosynaptic EPSPs in cat hindlimb motoneurones during fictive locomotion. *J Physiol* **526**, 639–652.

Granit R, Kernell D & Lamarre Y (1966*a*). Algebrical summation in synaptic activation of motoneurones firing within the primary range to injected currents. *J Physiol* **187**, 379–399.

Granit R, Kernell D & Lamarre Y (1966*b*). Synaptic stimulation superimposed on motoneurones firing in the 'secondary range' to injected current. *J Physiol* **187**, 401–415.

Graybill FA (1961). *An Introduction to Linear Statistical Models*. McGraw-Hill, New York.

Gustafsson B & Pinter J (1984). Relations among passive electrical properties of lumbar α-motoneurones of the cat. *J Physiol* **356**, 401–434.

Hansel D, Mato G & Meunier C (1993). Phase reduction and neural modeling. *Concepts Neurosci* **4**, 193–210.

Holt GR & Koch C (1997). Shunting inhibition does not have a divisive effect on firing rates. *Neural Comput* **9**, 1001–1013.

Hounsgaard J, Hultborn H, Jespersen B & Kiehn O (1988). Bistability of alpha-motoneurones in the decerebrate cat and in the acute spinal cat after intravenous 5-hydroxytryptophan. *J Physiol* **414**, 345–367.

Hultborn H, Enriquez-Denton M, Wienecke J & Nielsen JB (2003). Variable amplification of synaptic input to cat spinal motoneurones by dendritic persistent inward current. *J Physiol* **552**, 945–952.

Kernell D (1966). The repetitive discharge of motoneurones. In *Muscular Afferents and Motor Control*, ed. Granit R, pp. 351–362. John Wiley & Sons, New-York, London, Sydney; Almqvist & Wiksell, Stockholm.

Kernell D (1968). The repetitive impulse discharge of a simple neurone model compared to that of spinal motoneurones. *Brain Res* **11**, 685–687.

Kuo JJ, Lee RH, Johnson MD, Heckman HM & Heckman CJ (2003). Active dendritic integration of inhibitory synaptic inputs in vivo. *J Neurophysiol* **90**, 3617–3624.

Le Masson G, Renaud-Le Masson S, Debay D & Bal T (2002). Feedback inhibition controls spike transfer in hybrid thalamic circuits. *Nature* **417**, 854–858.

Manor Y, Yarom Y, Chorev E & Devor A (2000). To beat or not to beat: a decision taken at the network level. *J Physiol (Paris)* **94**, 375–390.

Mitchell SJ & Silver AR (2003). Shunting inhibition modulates neuronal gain during synaptic excitation. *Neuron* **38**, 433–445.

Nelson PG & Frank K (1967). Anomalous rectification in cat spinal motoneurons and effect of polarizing currents on excitatory post-synaptic potentials. *J Neurophysiol* **30**, 1097–1113.

Perreault M-C (2002). Motoneurons have different membrane resistance during fictive scratching and weight support. *J Neurosci* **22**, 8259–8265.

Poliakov AV, Powers RK & Binder MD (1997). Functional identification of the input-output transforms of motoneurones in the rat and cat. *J Physiol* **504**, 401–424.

Powers RK & Binder MD (1995). Effective synaptic current and motoneuron firing rate modulation. *J Neurophysiol* **74**, 793–801.

Powers RK & Binder MD (2001). Input-output functions of mammalian motoneurons. *Rev Physiol Biochem Pharmacol* **143**, 137–263.

Prinz AA, Abbott LF & Marder E (2004). The dynamic clamp comes of age. *Trends Neurosci* **27**, 218–224.

Robinson HP & Kawai N (1993). Injection of digitally synthesized synaptic conductance transients to measure the integrative properties of neurons. *J Neurosci Meth* **49**, 157–165.

Schwindt PC (1973). Membrane-potential trajectories underlying motoneuron rhythmic firing at high rates. *J Neurophysiol* **36**, 434–449.

Schwindt PC & Calvin WH (1973*a*). Equivalence of synaptic and injected current in determining the membrane potential trajectory during motoneuron rhythmic firing. *Brain Res* **59**, 389–394.

Schwindt PC & Calvin WH (1973*b*). Nature of conductances underlying rhythmic firing cat spinal motoneurons. *J Neurophysiol* **36**, 955–973.

Schwindt PC & Crill WE (1982). Factors influencing motoneuron rythmic firing: results from a voltage-clamp study. *J Neurophysiol* **48**, 875–890.

Shapovalov AI & Grantyn AA (1968). Suprasegmental synaptic effect on chromatolyzed motor neurons. *Biofizika* **13**, 260–269.

Sharp AA, O'Neil MB, Abbott LF & Marder E (1993). Dynamic clamp: computer-generated conductances in real neurons. *J Neurophysiol* **69**, 992–995.

Shefchyk SJ & Jordan LM (1985). Motoneuron input-resistance changes during fictive locomotion produced by stimulation of the mesencephalic locomotor region. *J Neurophysiol* **54**, 1101–1108.

Shriki O, Hansel D & Sompolinsky H (2003). Rate models for conductance-based cortical neuronal networks. *Neural Comput* **15**, 1809–1841.

Ulrich D (2003). Differential arithmetic of shunting inhibition for voltage and spike rate in neocortical pyramidal cells. *Eur J Neurosci* **18**, 2159–2165.

Zhang L & Krnjevic K (1987). Apamin depresses selectively the after-hyperpolarization of cat spinal motoneurons. *Neurosci Lett* **74**, 58–62.

Acknowledgements

Financial support provided by Délégation Générale pour l'Armement (DGA Grant 0034029) and by Ministère de la Recherche (Action Concertée Incitative 'Neurosciences Intégratives et Computationnelles') is gratefully acknowledged. We are indebted to Dr C. Capaday for stimulating discussions about this work. We wish to thank Drs M. Buiatti, L. Graham and L. Jami for helpful comments and M. Manuel and A. Roxin for carefully scrutinizing the manuscript.